

# TERASCALE BEAM-BEAM SIMULATIONS FOR TEVATRON, RHIC AND LHC\*

J. Qiang<sup>†</sup>, LBNL, Berkeley, CA 94547, USA

## Abstract

In this paper, we report on recent advances in terascale simulations of the beam-beam interaction in Tevatron, RHIC and LHC. Computational methods for self-consistent calculation of beam-beam forces are reviewed. A new method for solving the two-dimensional Poisson equation with open boundary conditions is proposed and tested. This new spectral-finite difference method is a factor of four faster than the widely used FFT based Green function method for beam-beam interaction on axis. We also present applications to the study of antiproton losses during the injection stage at Tevatron, to the study of multiple bunch coherent beam-beam modes at RHIC, and to the study of beam-beam driven emittance growth at LHC.

## INTRODUCTION

Beam-beam interaction plays an important role in high energy storage ring colliders. At interaction points, the nonlinear electromagnetic fields generated by one beam focus or defocus the opposite beam. This nonlinear beam-beam force can cause emittance growth and reduce the beam lifetime in the machine. An accurate modeling of the beam-beam interaction on terascale parallel computer will help to optimize the current machine operation and the future machine design.

To calculate the beam-beam force, a soft Gaussian approximation is sometimes used to obtain the electromagnetic fields of the beams at the collision point [1, 2, 3]. While this approximation has the advantage of computational speed, it is not self-consistent because it assumes a Gaussian distribution for the macroparticles even when the actual distribution might differ substantially from the Gaussian shape. To take into account the effects of the beam distribution self-consistently, one has to solve the Poisson equation numerically during each collision for the actual macroparticle distribution at that instant. A number of methods have been used to solve the Poisson equation. A five-point finite difference method with Fourier analysis and cyclic reduction (FACR) has been used by Krishnagopal [4] and Cai et al. [5]. This method solves the Poisson equation efficiently with finite domain boundary conditions. For the open boundary conditions, which are appropriate in typical beam-beam simulations, the method requires finding an effective boundary condition on the problem boundary; this can be computationally expensive. In addition, this method is not efficient to handle the case

with two widely separated beams, where the domain of the source particles (particle domain) and the domain of the electric field (field domain) are different. Another method based on the fast multipole expansion has been used by Herr et al. [6] to solve the Poisson equation. In this method, the computational cost scales linearly with the number of particles or with the number of total mesh points for the open boundary condition. The efficiency of this method is independent of the distribution of the source particles and the field domain, which makes it suitable to handle the situation with two separated beams. However, this method is an approximate algorithm in the sense that the accuracy of the expansion depends on the radius of convergence. The computational speed depends on the number of polynomials required in the multipole expansion.

A widely used method to solve the Poisson equation in beam-beam simulations is the Green function method with fast Fourier transform (FFT) on uniform grid [7, 8, 9, 10, 11]. In this method, the electric potential is written as a discrete convolution of the Green function and the charge density distribution. The original computational domain is doubled to construct a new periodic Green function and a new periodic charge density distribution. The convolution from the new Green function and charge density can be calculated very efficiently using the FFT method. This convolution gives the same electric potential inside the original domain [12]. The computational cost scales as  $N^2 \log(N)$ , where  $N$  is the number of grid points in each dimension. By defining a new shifted integrated Green function, this method can handle the separated beams, and beams with large aspect ratio [8, 13].

## SPECTRAL-FINITE DIFFERENCE SOLUTION OF THE POISSON EQUATION

The standard FFT based Green function method requires doubling the computational grid in both horizontal and vertical directions. This causes a factor of three increase of computational cost and storage. In the following, we will describe a new numerical method to solve the two-dimensional Poisson equation with open boundary conditions. We write the Poisson equation in cylindrical coordinates as:

$$\frac{\partial^2 \phi}{\partial r^2} + \frac{1}{r} \frac{\partial \phi}{\partial r} + \frac{1}{r^2} \frac{\partial^2 \phi}{\partial \theta^2} = -\rho/\epsilon_0 \quad (1)$$

Since both the electric potential and the charge density distribution are periodic function of  $\theta$ , we can approximate the

\* Work supported by a SciDAC project in accelerator physics which is supported by the US DOE/SC Office of High Energy Physics and the Office of Advanced Scientific Computing Research.

<sup>†</sup> jqiang@lbl.gov

potential  $\phi$  and the source term  $\rho$  as:

$$\rho_n(r, \theta) = \sum_{m=-N_m/2}^{N_m/2-1} \rho^m(r) \exp(-im\theta) \quad (2)$$

$$\phi_n(r, \theta) = \sum_{m=-N_m/2}^{N_m/2-1} \phi^m(r) \exp(-im\theta) \quad (3)$$

Substituting equations 2 and 3 into the original Poisson equation 1, we obtain a group of decoupled ordinary differential equations as:

$$\frac{\partial^2 \phi^m}{\partial r^2} + \frac{1}{r} \frac{\partial \phi^m}{\partial r} - \frac{m^2}{r^2} \phi^m = -\rho^m / \epsilon_0 \quad (4)$$

The solution of above equation outside the particle domain has the form:

$$\phi(r) = cr^{-m}, \quad m > 0 \quad (5)$$

$$\phi(r) = c \log(r), \quad m = 0 \quad (6)$$

Inside the particle domain, using a second-order finite difference scheme, we obtain

$$\left(\frac{1}{h^2} + \frac{1}{hr_n}\right)\phi_{n+1}^m - \left(\frac{2}{h^2} + \frac{m^2}{r_n^2}\right)\phi_n^m + \left(\frac{1}{h^2} - \frac{1}{hr_n}\right)\phi_{n-1}^m = -\frac{\rho_n^m}{\epsilon_0} \quad (7)$$

where  $n$  is an integer between 0 ( $m > 0$ ) or 1 ( $m = 0$ ) and maximum grid number  $N$ . Matching the solution outside the particle domain with the solution inside the domain at maximum grid  $N$ , we obtain

$$\phi_{N+1} = \phi_N (r_N / r_{N+1})^m, \quad m > 0 \quad (8)$$

$$\phi_{N+1} = \phi_N \log(r_{N+1}) / \log(r_N), \quad m = 0 \quad (9)$$

Together with the boundary condition at  $r = 0$ , it forms  $N + 2$  ( $m > 0$ ) and  $N + 1$  ( $m = 0$ ) tri-diagonal linear algebra equations which can be solved with order of  $N$  operations.

As a test example of above algorithm, we have computed the electric field for a Gaussian density beam with horizontal to transverse aspect ratio of five. Fig. 1 shows the horizontal electric field along positive horizontal axis together with the analytical solution. Fig. 2 shows the vertical electric field along positive vertical axis together with the analytical solution. We see that the numerical solutions and the analytical solutions agree with each other very well.

## APPLICATIONS TO TEVATRON, RHIC AND LHC BEAM-BEAM STUDIES

As the first example of applications, we have done parameter scan study of antiproton losses during the injection stage with energy of 150 GeV in the Tevatron [14]. In the simulation, we have assumed a strong-weak beam-beam interaction model since the antiproton intensity is much smaller than the proton intensity (typically a factor of 10).

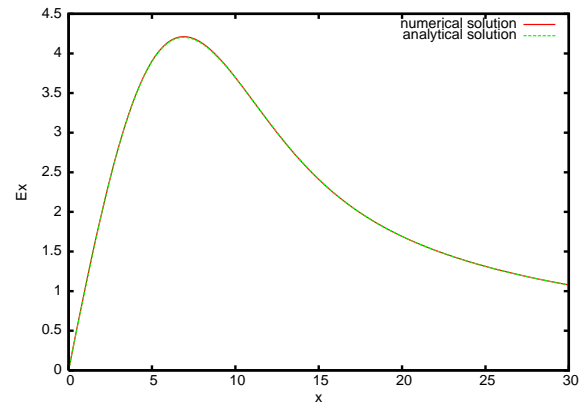


Figure 1: Horizontal electric field along the positive horizontal axis together with analytical solution.

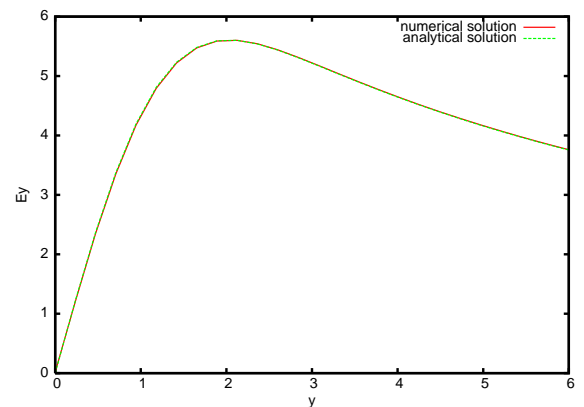


Figure 2: Vertical electric field along the positive vertical axis together with analytical solution.

We have also assumed an ‘‘aperture’’ size of  $3.25\sigma$ , where the  $\sigma$  is the horizontal or vertical rms size at each collision point. The choice of the aperture size is based on the particle tracking study of the dynamic aperture in the Tevatron [15]. The noise amplitude is set as  $2 \times 10^{-8}$  which gives a few pi-mm-mrad antiproton emittance growth after one hour machine operation. Fig. 3 shows a plot of the antiproton losses at the injection energy of 150 GeV with different proton intensities from the simulation. It is seen that with increasing proton intensity, more antiproton gets lost. This is in qualitative agreement with the experimental observation.

The second example of applications is to study coherent modes of multi-bunch collisions at RHIC through strong-strong beam-beam simulations. Fig. 4 gives a schematic plot of two colliding beams at RHIC. Here each beam has three bunches. The six bunches couple with each other through collisions at four interaction points, IP2, IP6, IP8 and IP10. The coherent modes of multi-bunch beam-beam interaction are first studied using a rigid beam approximation since the mode frequency can be checked with the analytical calculation [16]. Fig. 5 shows power spectra of hor-

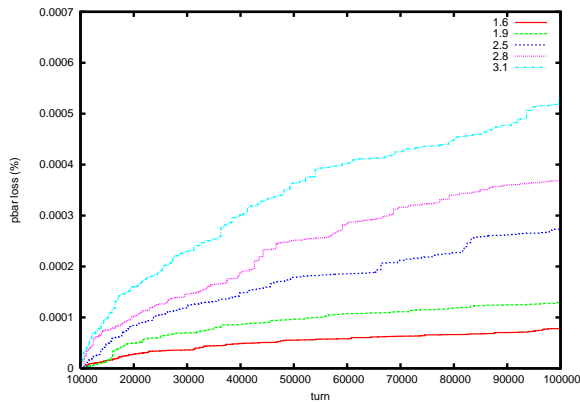


Figure 3: Normalized antiproton intensity evolution for different proton intensities.

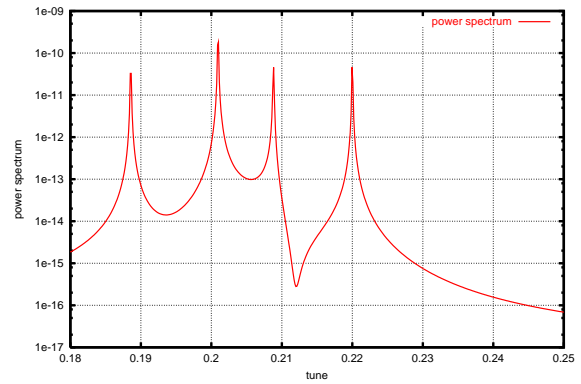


Figure 5: Power spectra (arbitrary normalization) of the horizontal centroid motion of one bunch at RHIC from a rigid beam approximation.

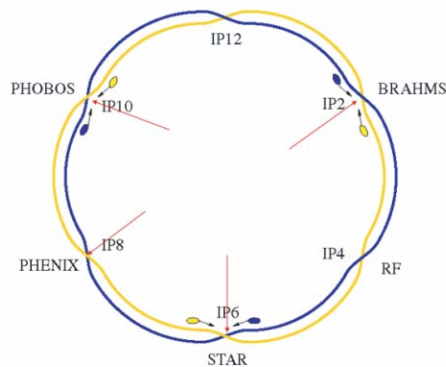


Figure 4: A schematic plot of two colliding beams at RHIC.

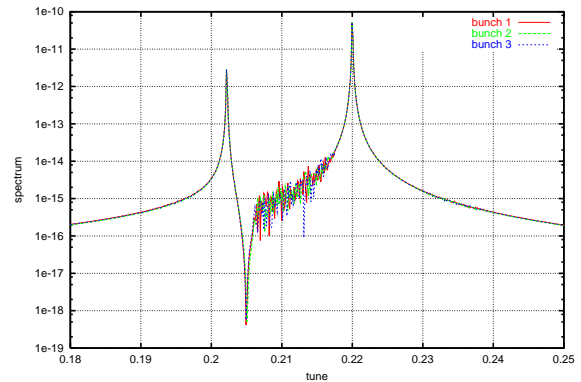


Figure 6: Power spectra (arbitrary normalization) of the horizontal centroid motion of three bunches at RHIC.

horizontal centroid motion of one bunch from a rigid beam approximation. There are only four coherent modes observed from the simulation instead of six eigenmodes. The degeneration of the eigenmodes is due to the symmetric structure of the collision at RHIC. This is also verified from the analytical calculation. Fig. 6 shows power spectra of horizontal centroid motion of three bunches from self-consistent strong-strong beam-beam simulation. There are only two distinct eigenmodes, the  $\pi$  mode (180 degree out of phase) and the  $\sigma$  mode (in phase), which are observable in this example. The other four modes are degenerated and buried into the incoherent continuous spectra. The  $\pi$  mode tune shift is  $4.918\xi$  which is about of a factor of 4 times the single bunch  $\pi$  tune shift  $1.21\xi$ . This is in agreement with the analytical calculation of Yokoya et. al. [17]. The large tune shift of the  $\pi$  mode due to the multi-bunch collisions presents a potential instability since it can not be damped out by the continuous spectra through the Landau damping. In above example, we have assumed that the two beams have the same parameters. In reality, the parameters of two rings can be controlled so that the two colliding beams have

different tunes. Fig. 7 gives power spectra of horizontal centroid motion of three bunches with the horizontal tune of the second beam set as 0.2 while the first beam is set as 0.22. The two colliding beams lose the coherent motion and the dipole mode disappears into the continuous spectra.

The third example of applications is to study the emittance growth and halo formation driven by the mismatched and time-modulated beam-beam interaction at LHC. We have tracked the macroparticles for one million turns to be related to the real machine measurement which is normally done on the order of minutes. Here, one million turns at LHC corresponds to about 1.5 minutes. Unfortunately, for such a long time simulation, the emittance growth driven by numerical collisionality of finite macroparticle noise is no longer negligible. To understand and to control this effect, we have done simulations using different charge deposition and field interpolation schemes, different numerical mesh size, different number of macroparticles for the nominal LHC beam-beam parameters. Here, we have included only one head-on collision in the simulation. Fig. 8 shows the averaged emittance growth using a linear depo-

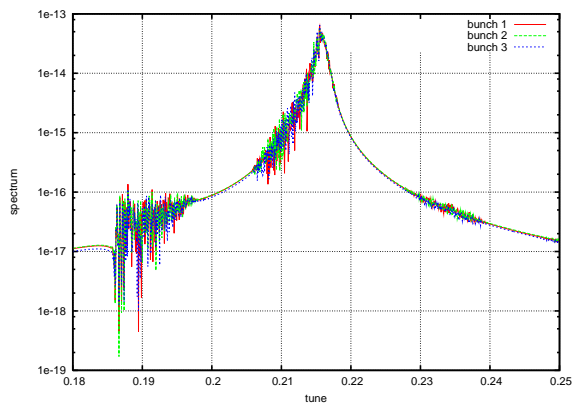


Figure 7: Power spectra (arbitrary normalization) of the horizontal centroid motion of three bunches with different tune in each ring of RHIC.

sition/interpolation, a quadratic deposition/linear interpolation, and a quadratic deposition/interpolation scheme. It

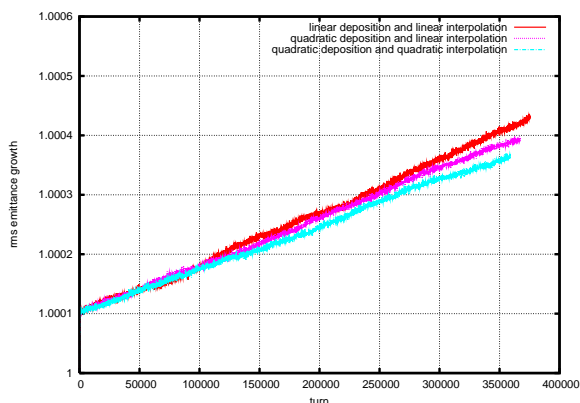


Figure 8: Averaged emittance growth with linear and quadratic deposition/interpolation scheme.

is seen that the quadratic charge deposition and quadratic field interpolation gives the lowest emittance growth. This is because the quadratic deposition/interpolation generates a smoother density and field data than the linear deposition/interpolation, which reduces macroparticle noise in the simulation. On the other hand, the macroparticle noise can also be reduced using a coarser computational grid. This corresponds to a larger size of macroparticle. Fig. 9 shows the averaged emittance growth using  $128 \times 128$  and  $64 \times 64$  grid points. Using a coarser grid does help to reduce the numerical emittance growth driven by the macroparticle noise. The number of macroparticles used also affects the numerical collisional noise. With more macroparticle used, the charge of each macroparticle is closer to that of a real particle, and the numerical collisional noise gets smaller. Fig. 10 shows the averaged emittance growth with 0.5 million, 1 million and 2 million macroparticles. It is seen that with more macroparticles, the numerical emittance growth

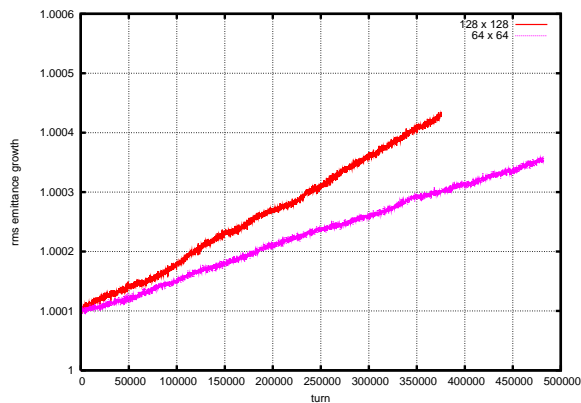


Figure 9: Averaged emittance growth with  $128 \times 128$  and  $64 \times 64$  grid points.

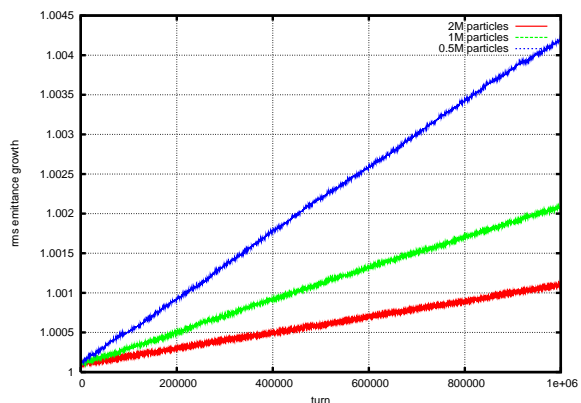


Figure 10: Averaged emittance growth with 0.5M, 1M and 2M macroparticles.

has dropped significantly. The emittance growth in this figure is characterized by a least square fitting of the emittance growth as a function of time (in the unit of turn) and macroparticle number:

$$\epsilon(t)/\epsilon(0) = 1.0001 + 0.00257/N^{1.0175}T \quad (10)$$

This suggests that the numerical emittance growth is about inversely proportional to the macroparticle number. In this figure, we have used a linear deposition/interpolation scheme with  $256 \times 256$  grid points. These factors will also affect the numerical emittance growth as we discussed before.

A sweeping beam detector has been proposed as a device to monitor and to optimize the luminosity at the LHC. In this scheme, one of the beams is deliberately made to rotate about a fixed axis as it collides with the opposite beam. To study the emittance growth for such time-modulated beam-beam interaction, we have carried out a strong-strong simulation using 0.25 million particles, 0.5 million particles, 1 million particles and 2 million particles for 1 million turns. The average emittance growth after 1 million

turns as a function of macroparticle number is shown in Fig. 11. The real emittance growth after one million turns

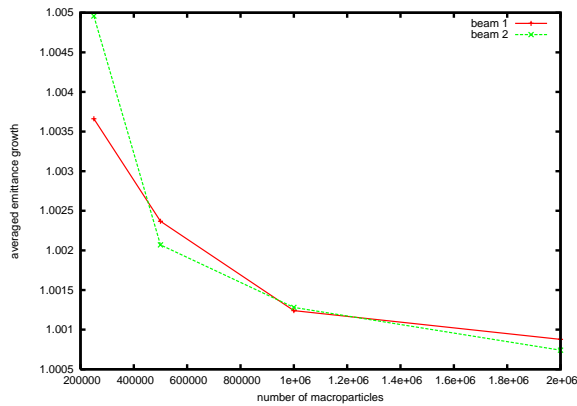


Figure 11: Emittance growth as a function of number of macroparticles after 1M turns.

can be estimated from the extrapolation, which gives about 0.05% emittance growth. It can be seen that for a quarter million macroparticles, the numerical emittance growth is much higher than the real emittance growth.

When two beams collide with a mismatch of beam size, the large amplitude particles of one beam receive strong nonlinear forces from the opposite beam. This could cause the growth of tail particles to form a halo. In high intensity beam study, 99.9% emittance has been used to characterize the halo distribution. Here, 99.9% emittance is defined as the emittance which contains 99.9% particles [18]. Fig. 12 shows the averaged 99.9% emittance evolution from the beam-beam interaction with equal beam size and 10% mismatched beam size. We see that the mismatched beam-

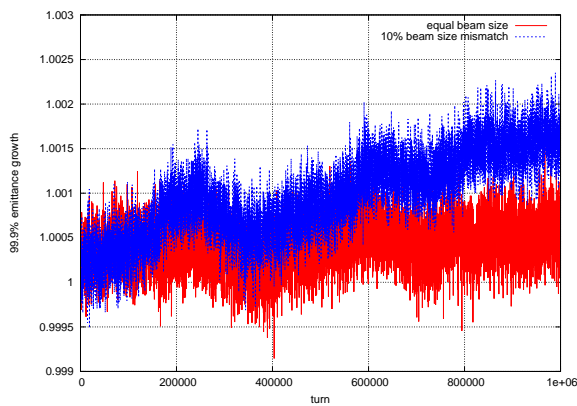


Figure 12: 99.9% emittance growth with equal beam size and with 10% beam size mismatch.

beam interaction has resulted in a larger emittance growth than the nominal case. This might be due to some high order resonance observed at SPS collider [19].

## ACKNOWLEDGMENTS

We would like to thank Drs. M. Xiao and W. Fischer for Tevatron and RHIC beam-beam lattice information and discussions. We also thank Drs. M. Furman, R. Ryne, W. Turner, M. Zisman, T. Sen, P. Spentzouris, V. Shiltsev, W. Herr and F. Zimmermann for constructive comments. This research used resources of the National Energy Research Scientific Computing Center, and the resources of the Center for Computational Sciences at OAK Ridge National Laboratory.

## REFERENCES

- [1] K. Hirata, H. Moshhammer and F. Ruggiero, *Particle Accelerators* **40**, 1993, p. 205.
- [2] M. A. Furman, "Beam-Beam Simulations with the Gaussian Code TRS", LBNL-42669, CBP Note 272, 1999.
- [3] M. P. Zorzano and F. Zimmermann, *Phys. Rev. Special Topics - Accel. Beams* **3**, April 2000, 044401.
- [4] S. Krishnagopal, *Phys. Rev. Lett.* **76**, 1996, pp. 235-238.
- [5] Y. Cai, A. W. Chao, S. I. Tzenov, and T. Tajima, *Phys. Rev. Special Topics - Accel. Beams* **4**, Jan. 2000, 011001.
- [6] W. Herr, M. P. Zorzano, and F. Jones, *Phys. Rev. Special Topics - Accel. Beams* **4**, May 2001, 054402.
- [7] E. B. Anderson, T. I. Banks, J. T. Rogers, in *Proceedings of the 1999 Particle Accelerator Conference*, New York, 1999, pp. 1686-1688.
- [8] K. Ohmi, *Phys. Rev. E* **62**, 2000, pp. 7287-7294.
- [9] J. Shi and D. Yao, *Phys. Rev. E* **62**, 2000, pp.1258-1265.
- [10] J. Qiang, M. A. Furman, and R. D. Ryne, *Phys. Rev. Special Topics - Accel. Beams* **5**, 2002, 104402.
- [11] A. Kabel, in *Proc. of the 2003 Particle Accelerator Conference*, Portland, 2003, pp. 3545-3547.
- [12] R. W. Hockney and J. E. Eastwood, *Computer Simulation Using Particles*, McGraw-Hill, New York, 1985.
- [13] J. Qiang, M. A. Furman, and R. D. Ryne, *J. Comp. Phys.* **198**, 2004, pp. 278-294.
- [14] J. Qiang, et al., in *Proc. of the 2003 Particle Accelerator Conference*, Portland, 2003, pp. 3401-3403.
- [15] M. Xiao, T. Sen, and B. Erdelyi, in *Proc. of the 2003 Particle Accelerator Conference*, Portland, 2003, pp. 1772-1774.
- [16] A. W. Chao, in *Nonlinear Dynamics and the Beam-Beam Interaction*, AIP Conf. Proceedings, No. 57, ed. by M. Month and J. C. Herrera, (1980), p. 42.
- [17] K. Yokoya and H. Koiso, *Part. Accel.* **27**, 1990, p. 181.
- [18] T. P. Wangler, *Principles of RF Linear Accelerators*, John Wiley & Sons, New York, 1998.
- [19] W. Herr, in *Proc. of a Workshop on Beam-Beam Effects in Circular Colliders*, Fermilab, June 25-27, (2001), p. 6.